The Astrophysical Journal Letters, 770:L27 (5pp), 2013 June 20 doi:10.1088/2041-8205/770/2/L27

ALMA FOLLOWS STREAMING OF DENSE GAS DOWN TO 40 pc FROM THE SUPERMASSIVE BLACK HOLE IN NGC 1097

Kambiz Fathi[1,2], Andreas A. Lundgren[3], Kotaro Kohno[4,5], Nuria Piñol-Ferrer[1], Sergio Martín[6], Daniel Espada[7], Evanthia Hatziminaoglou[8], Masatoshi Imanishi[9], Takuma Izumi[4], Melanie Krips[10], Satoki Matsushita[11], David S. Meier[12,13], Naomasa Nakai[14], Kartik Sheth[15], Jean Turner[16], Glenn van de Ven[17], and Tommy Wiklind[3]
[1] Stockholm Observatory, Department of Astronomy, Stockholm University, AlbaNova Centre, 106 91 Stockholm, Sweden
[2] Oskar Klein Centre for Cosmoparticle Physics, Stockholm University, 106 91 Stockholm, Sweden
[3] Joint ALMA Observatory, Alonso de Córdova 3107, Vitacura, Santiago, Chile
[4] Institute of Astronomy, The University of Tokyo, 2-21-1 Osawa, Mitaka, Tokyo 181-0015, Japan
[5] Research Center for the Early Universe, The University of Tokyo, 7-3-1 Hongo, Bunkyo, Tokyo 113-0033, Japan
[6] ESO, Alonso de Córdova 3107, Vitacura, Santiago, Chile
[7] National Astronomical Observatory of Japan (NAOJ), 2-21-1 Osawa, Mitaka, Tokyo 181-8588, Japan
[8] ESO, Karl-Schwarzschild-Str. 2, D-85748 Garching bei München, Germany
[9] Subaru Telescope, National Astronomical Observatory of Japan, 650 North A'ohoku Place, Hilo, HI 96720, USA
[10] Institute for Radio-Astronomy at Millimeter Wavelengths, Domaine University, 300 Rue de la Piscine, F-38406 Saint Martin d'Heres, France
[11] Academia Sinica, Institute of Astronomy and Astrophysics, P.O. Box 23-141, Taipei 10617, Taiwan (ROC)
[12] Department of Physics, New Mexico Institute of Mining and Technology, 801 Leroy Place, Socorro, NM 87801, USA
[13] National Radio Astronomy Observatory, P.O. Box O, Socorro, NM 87801, USA
[14] Division of Physics, Faculty of Pure and Applied Science, University of Tsukuba, Tsukuba, Ibaraki 305-8571, Japan
[15] National Radio Astronomy Observatory, 520 Edgemont Road, Charlottesville, VA 22903, USA
[16] Department of Physics and Astronomy, UCLA, Los Angeles, CA 90095-1547, USA
[17] Max Planck Institute for Astronomy, Königstuhl 17, D-69117 Heidelberg, Germany
Received 2013 February 2; accepted 2013 April 24; published 2013 June 3

ABSTRACT

We present a kinematic analysis of the dense molecular gas in the central 200 pc of the nearby galaxy NGC 1097, based on Cycle 0 observations with the Atacama Large Millimeter/submillimeter Array (ALMA). We use the HCN(4–3) line to trace the densest interstellar molecular gas ($n_{H_2} \sim 10^8$ cm^{-3}), and quantify its kinematics, and estimate an inflow rate for the molecular gas. We find a striking similarity between the ALMA kinematic data and the analytic spiral inflow model that we have previously constructed based on ionized gas velocity fields on larger scales. We are able to follow dense gas streaming down to 40 pc distance from the supermassive black hole in this Seyfert 1 galaxy. In order to fulfill marginal stability, we deduce that the dense gas is confined to a very thin disk, and we derive a dense gas inflow rate of 0.09 $M_\odot$ yr^{-1} at 40 pc radius. Combined with previous values from the Hα and CO gas, we calculate a combined molecular and ionized gas inflow rate of ~0.2 $M_\odot$ yr^{-1} at 40 pc distance from the central supermassive black hole of NGC 1097.

Key words: galaxies: active – galaxies: individual (NGC 1097) – galaxies: kinematics and dynamics

Online-only material: color figures

1. INTRODUCTION

The central region of the nearby barred Seyfert 1 galaxy NGC 1097 displays a number of intriguing morphological and kinematic features. At ~1 kpc, an almost circular ring-like feature marks the transition between the prominent $R \sim 8$ kpc galactic bar and the relatively diffuse region interior to the ring. The bar hosts two prominent dust lanes, both originating at around the corotation radius of the bar (Piñol-Ferrer et al. 2013), cutting through the inner ring and transforming into nuclear spirals that continue down to ~3.5 pc distance from the active nucleus (Lou et al. 2001; Fathi et al. 2006). The dust lanes are accompanied by diffuse ionized gas revealing clear kinematic signatures of bar-induced gas inflow over the entire face of the galaxy (Piñol-Ferrer et al. 2013).

Neutral gas and ionized gas data cubes (Ondrechen et al. 1989; Fathi et al. 2006) have confirmed the "abundant" presence of these two phases of the interstellar medium across the central kpc radius. However, interferometric molecular gas maps show emission confined to the nuclear ring and the central 200–300 parsecs radius (Kohno et al. 2003; Hsieh et al. 2008, 2011, 2012). Moreover, Piñol-Ferrer et al. (2011) showed that the bulk of the interstellar gas at the center of NGC 1097 (like in many other galaxies) is in the molecular phase, and therefore, a detailed analysis of the central gas concentration needs to account for the different physical conditions. The interplay between the different phases provide crucial clues for understanding the energies involved in redistributing the gas in a way that leads to the observed phase transition efficiencies.

The discovery of broad (~10,000 km s^{-1}) double-peaked Hα emission lines by Storchi-Bergmann et al. (1993) makes NGC 1097 also an ideal laboratory for studying the fate of the gas accumulated in the centers of active galactic nuclei (AGNs). At a distance of 14.5 Mpc (i.e., ~70 pc arcsec^{-1}), this galaxy is also suitable for high-resolution studies of the physical processes that cause the material/fuel to loose its angular momentum and fall toward the AGN (e.g., Storchi-Bergmann et al. 2003).

Although it is straightforward to transport gas down to the central kpc and induce enhanced star formation, it is more difficult to make the gas reach smaller scales (few pc) required to fuel an AGN. In rotating systems, perturbations can cause the potential to become non-axisymmetric, and torques exerted by the subsequent non-axisymmetric features are able to drive material toward the center (Schwarz 1984). Sheth & Teuben (1999) have argued that magnetic stress may aid the infalling

gas to complete the last few parsecs down to the central supermassive black hole (SMBH).

To build a realistic scenario for the fate of the gas that is piling up around an AGN to eventually fuel it, one has to make a detailed analysis of the distribution and kinematics of multiple phases of the interstellar gas in the region of interest.

Based on ionized gas kinematic maps (van de Ven & Fathi 2010, hereafter vdVF; Piñol-Ferrer et al. 2013), we have derived a concise picture for NGC 1097, according to which the gravitational perturbation that once gave rise to the formation of the prominent bar drives the evolution of structure inside the bar as well as the outer spiral arms. The outer spiral arms are confined between the corotation radius and reach beyond the outer Lindblad resonance radius of the main galactic bar. The circumnuclear ring once formed at the location of the outer inner Lindblad resonance (Piñol-Ferrer et al. 2013), and has likely migrated toward the center of the galactic gravitational potential (Regan & Teuben 2003; van de Ven & Chang 2009). Inside the ring, the non-circular velocities are consistent with the presence of two spiral arms (in morphology). The nuclear arms are well disguised in optical images, and several image-enhancement techniques have led different authors to argue for a different number of arms (e.g., Lou et al. 2001; Davies et al. 2009; vdVF). Most of the disagreements concern the inner ∼100 pc, where increased dust content may have distorted both images and kinematic measurements in the optical and near-infrared.

Here we present a quantitative analysis of the kinematics of the densest molecular gas within the central kpc radius of NGC 1097 based on Atacama Large Millimeter/submillimeter Array (ALMA) observations of hydrogen cyanide, HCN(4–3) (Proposal 2011.0.00108.S, PI: Kohno). We compare the ALMA kinematic data with a dynamical model that we have previously constructed based on two-dimensional spectroscopic data of ionized gas.

2. THE DATA

NGC 1097 was observed with ALMA on 2011 November 5–6, with 14 and 15 antennas, respectively. Our Band 7 observations targeted the HCN(4–3) line at rest frequency of 354.505 GHz with the original channel spacing of 488.28125 kHz. To increase the signal strength, the data were binned by a factor 20, leading to an effective channel width of 9.77 MHz (∼8.3 km s^{-1}). The primary beam was 18.″1 with a synthesized beam of 1.″50 × 1.″20 (∼105 × 84 pc) and at −72.°4 position angle (P.A.), sampled at 0.″3 pixel^{-1}. All data specifications are described in Izumi et al. (2013).

Figure 1 shows the integrated intensity map of HCN(4–3) with the velocity moment maps and models, described below. At this resolution the spiral arms are difficult to see in the integrated intensity map, which sums all velocities, but are easier to detect in the kinematics.

The HCN(4–3) kinematics were derived in two ways. The simple first moment map (intensity-weighted mean velocity map) was cross checked with Gaussian fitting to each individual spectrum. We found no significant signatures of non-Gaussianity; however, the Gaussian fits resulted in a generally noisier velocity field. We use the moment 1 maps and exclude all pixels for which the corresponding spectrum amplitude-over-noise $A/N < 20$ (see Figure 1). We find almost no signal outside the area illustrated in Figure 1 at lower A/N values. This confirms that the dense gas is confined to a small region around the AGN in NGC 1097 (Hsieh et al. 2012).

The ratio between the Einstein coefficient and collisional rates for the HCN(4–3) transition results in an estimated critical density of a few times 10^7–10^8 cm^{-3} with a small dependency on temperature. Our calculation is conformal with previously reported densities of $n_{\rm H_2} \sim 10^8$ cm^{-3} at 40 K kinetic temperature (e.g., Choi et al. 2000; Takakuwa et al. 2007). Such high densities are also consistent with the deep obscuration expected toward the center of a galaxy (e.g., Kohno et al. 1996; Sakamoto et al. 2010).

To constrain the large-scale gas kinematics, we have used a mosaic of Fabry–Perot interferometric observations at 0.″83 spatial sampling, covering a 7′ × 7′ field at 15 km s^{-1} spectral resolution (Dicaire et al. 2008; Piñol-Ferrer et al. 2013). To further look into the central few 100 pc, we used Hα two-dimensional velocity field, at 0.″1 spatial sampling and 85 km s^{-1} spectral resolution, from the Gemini South Telescope's Integral Field Unit, covering the inner 7″ × 15″ (Fathi et al. 2006). The combination of the two sets of data is imperative, as they present a coherent dynamical model for NGC 1097 from ∼20 kpc down to ∼100 pc from its central SMBH.

3. KINEMATIC PARAMETERS

We assume that the galactic disk is predominantly rotating and apply the prescription used in vdVF to quantify the velocity field shown in the top middle panel of Figure 1. We divide the observed velocity field into concentric rings, each containing >7 pixels (this sets the limit for the innermost radius to 0.″55 $\lesssim$ 40 pc). We fix the inclination at 35° and apply a χ^2 minimization to obtain the central coordinates (x_0, y_0), systemic velocity $V_{\rm sys}$, and P.A. of the disk. After fixing these parameters, we make the final χ^2 fit to the desired modes (here up to and including third order) of the Fourier decomposition mathematically formulated as

$$V_{\rm los} = V_{\rm sys} + \sum_{n=1}^{k} [c_n(r)\cos n\theta + s_n(r)\sin n\theta]\sin i. \quad (1)$$

We apply Equation (1) to the HCN(4–3) velocity field and find an agreement between the kinematic and photometric center to within one pixel (see Figure 1). Each ring is populated at more than 225°; hence, we ensure that we do not need to assume any level of symmetry in the observed non-circular motions. We derive a systemic velocity of 1300 ± 48 km s^{-1} and the kinematic P.A. of $147° \pm 6°$. In Figure 1 we illustrate the different stages of the fits described here, and a three-fold symmetry can be found in the non-circular velocity field (as predicted for this region in NGC 1097 by vdVF). The average final residual velocities are 10 km s^{-1}, indicating that we have reproduced 95% of the observed velocity features with the Fourier decomposition method.

Fitting Gaussians to each spectrum gives us the average velocity uncertainty for all the pixels at 15 km s^{-1}. These errors are used to derive the uncertainties for the derived kinematics by means of Monte Carlo simulations. Repeated application to the Gaussian-randomized velocity field yields uncertainties on the Fourier parameters. Our simulations show that the average rotation curve uncertainty is 20% (see also Fathi et al. 2005). Similarly, the higher Fourier term uncertainties have been calculated, and we plot the first, second, and third Fourier terms of the HCN(4–3) data together with those derived from the GMOS data in Figure 2.

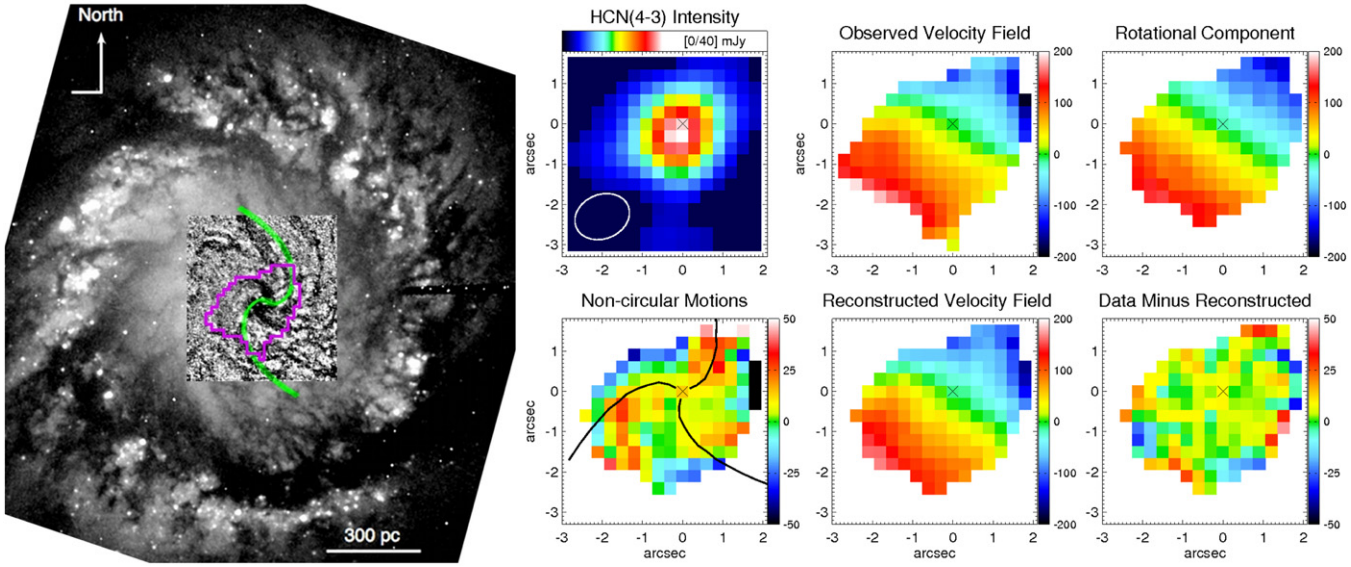

Figure 1. Left: *Hubble Space Telescope* (*HST*) Hα image with a structure map showing the nuclear dust features (Fathi et al. 2006) and the footprint of the ALMA HCN(4–3) pixels with $A/N \geqslant 20$ (magenta contours). Overplotted in green are the spiral arms modeled by vdVF. Right: ALMA HCN(4–3) distribution and velocity field. The circular and non-circular motion maps, Fourier reconstructed, and final residual maps are displayed in km s^{-1}. The black curves in the bottom left panel outline the predicted location of the non-circular motions due to the model spiral arms corresponding to the two-arm morphological arms drawn on the *HST* image (in green). The non-circular velocities follow a similar three-fold symmetry. The ellipse in the top left panel displays the beam size, and the cross marks the kinematic center, offset from the peak centroid by less than 0.″3.

(A color version of this figure is available in the online journal.)

4. ANALYSIS

The ionized gas velocity Fourier terms were modeled by vdVF, who constrained the detailed structure of the nuclear spiral arms and the associated gas inflow from kinematic data (solid curves in the lower panels of Figure 2). Their nuclear spiral structure is consistent with a weak perturbation in the gravitational potential due to a two-arm logarithmic spiral (in morphology) with a pitch angle of $52^{\circ} \pm 4^{\circ}$ derived directly from the Fourier expansion of the model velocity field. Similarly, large pitch angles in the very central parts of galaxies have also been modeled by Yuan & Yang (2006). Furthermore, the innermost ∼100 pc radius of the data points analyzed by vdVF displayed the largest errors in the third Fourier terms, as a consequence of dust contamination.

We test the effect of beam smearing on the derived kinematic parameters by artificially smoothing by a factor two, and find that the Fourier terms remain virtually unchanged. A notable effect of beam smearing is that it may lead to incorrect kinematic center, which in turn may cause uncertainties in the third Fourier terms. Wong (2000) found that smearing of 10″ could produce up to 10 km s^{-1} third Fourier terms. This is less than our error bars. In light of these tests and following the discussion in Wong (2000, Chapter 2), it unlikely that the innermost values would be affected by beam smearing.

In Figure 2, we overplot the ALMA HCN(4–3) velocity Fourier components on those derived from the GMOS data. The top panel reveals a very good agreement between the rotation curve ($\sim c_1$ in Equation (1)) of HCN(4–3) and that of the Hα gas in the central 200 pc. Hence, due to the agreement of their overall kinematics, the bulk rotation of the dense gas is coplanar to the ionized interstellar gas. Further light can be shed on the dynamical behavior of HCN(4–3) by considering the higher Fourier terms. Figure 2 illustrates the analytic spiral model that has lead to the kinematic derivation of the pitch angle of the nuclear spirals with associated gas inflow rates (vdVF; Piñol-Ferrer et al. 2011). A simple overplot of the ALMA data (filled circles) displays striking agreement between the relatively non-contaminated HCN(4–3) kinematic behavior and the model predictions. *The analytic spiral model predicts the HCN(4–3) velocity Fourier terms down to* $0.''55 \lesssim 40$ *pc.*

Besides the $n = 1$ and $n = 3$ Fourier terms in the velocity field, the non-circular motions also contain marginal $n = 2$ terms. vdVF argued that the $n = 2$ terms in the Hα were most likely due to dust contamination and possible shocks associated with the gas streaming along the nuclear spiral arms (see also Valotto & Giovanelli 2004). This seems to be confirmed here with the HCN(4–3) second terms consistent with zero inside 100 pc radius.

5. DENSE GAS STREAMING DOWN TO $\lesssim$40 pc FROM THE SMBH

We use the derived c_1 curve to measure the dynamical mass, assuming a thin disk model and velocity uncertainties of 20%. We derive the mass within the central 100 pc to $3.5^{+1.6}_{-2.0} \times 10^8\ M_{\odot}$, and inside the 40 pc radius, $8.0^{+2.9}_{-3.5} \times 10^6\ M_{\odot}$. These masses are based on velocity measurements well outside the sphere of influence of the SMBH (∼13 pc; Peebles 1972). Even so, in theory, a significant contribution from the SMBH is expected on the rotating velocities at 40 pc radius. However, the synthesized beam size of the ALMA data almost entirely smears out the effect of the SMBH at this radius, and therefore, a rotation curve at higher spatial resolution is needed to measure the dynamical mass of the SMBH. Furthermore, it should be noted that our mass estimate from the observed cold molecular gas rotation curve is not corrected for the contribution of non-circular motions in the c_1 curve (see Figure 3 in vdVF). Thus, these are likely lower mass limits.

The prescription for deriving mass inflow rates along the nuclear spirals has been presented in vdVF. They combined the resulting inflow velocity corresponding to the model spiral

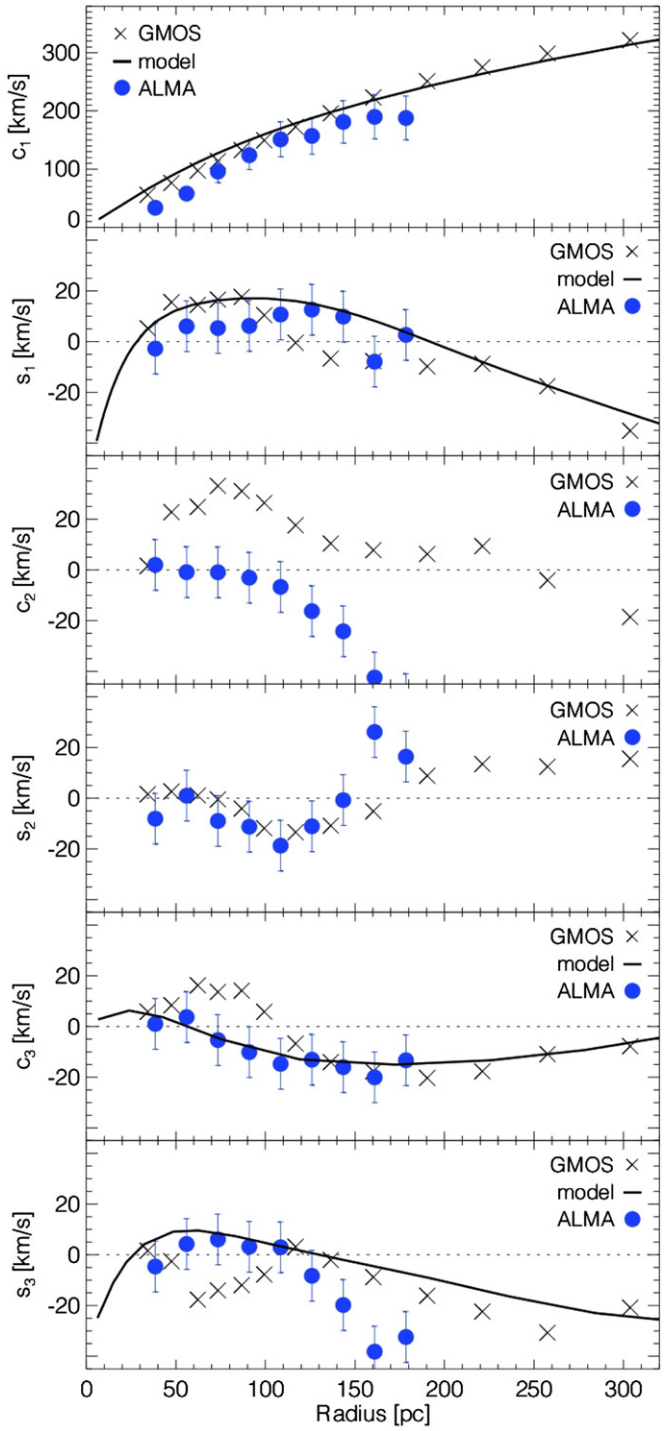

Figure 2. Comparing the quantified kinematics of the ionized gas in the optical (crosses) and the HCN(4–3) ALMA data (filled circles) to the analytic model prediction presented in vdVF. The spiral model is not a fit to any of the two data sets shown here, but a carefully chosen set of spiral parameters that best match the GMOS data. The HCN(4–3) data points are simple overplots of the new ALMA data showing a striking agreement with the model predictions. The model does not contain c_2 or s_2 terms (see Equations (A12) and (A13) in vdVF).

(A color version of this figure is available in the online journal.)

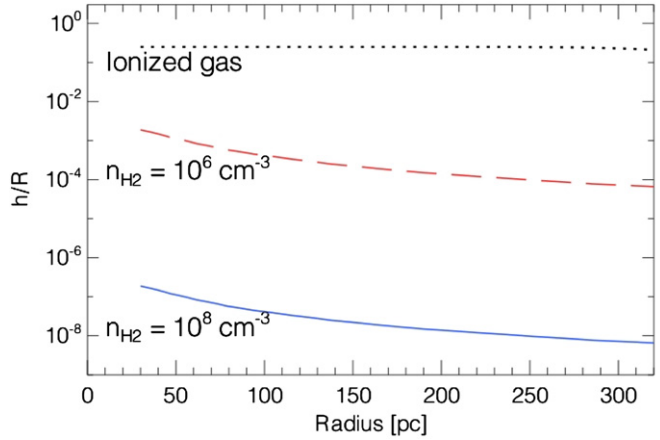

Figure 3. Disk scale height over radius h/R as a function of radius for the HCN(4–3) emitting gas at $n_{H_2} \sim 10^8$ (solid curve). For comparison, we also illustrate this parameter for the ionized gas (dotted curve) and the molecular counterparts at lower densities (dashed curve).

(A color version of this figure is available in the online journal.)

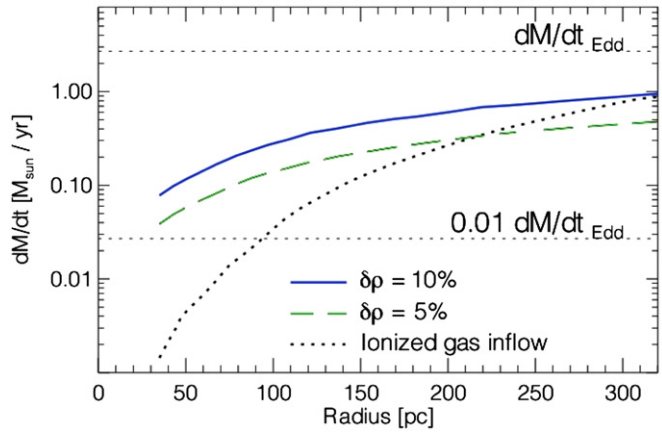

Figure 4. Dense gas inflow rate derived from the analytic spiral model of vdVF as a function of galactocentric radius. Changing the molecular gas density by two orders of magnitudes does not change the inflow rate curves; however, the arm vs. inter-arm overdensity $\delta\rho$ changes the inflow rate as illustrated by the solid and dashed curves.

(A color version of this figure is available in the online journal.)

arm parameters, with the gas density in the spiral arms inferred from [S II] emission line ratios. They calculated the ionized gas inflow rate as a function of radius, reaching 0.033 $M_\odot$ yr^{-1} at a distance of 100 pc from the central SMBH. The inflow rate was later refined by Piñol-Ferrer et al. (2011), who used CO gas measurements to derive one order of magnitude higher molecular gas inflow rate for a marginally stable disk model. Using this formalism, Piñol-Ferrer et al. (2011) derived the CO gas inflow of 0.3 $M_\odot$ yr^{-1} at 100 pc radius.

As we compare the HCN(4–3) kinematics with our previous results for ionized and CO gas (vdVF; Piñol-Ferrer et al. 2011), we set the sound speed at 10 km s^{-1} and derive the dense gas scale height (Figure 3) using the observed epicyclic frequency. We then use the kinematic parameters from the analytic spiral model to trace the gas inflow down to the resolution limit ($0\farcs55 \lesssim 40$ pc). The data set at hand does not allow us to investigate the density difference between the nuclear spiral arms and the inter-arm region in NGC 1097. We assume 10% overdensity, similar to the upper limit of the observed value from the [S II] doublet, and in agreement with numerical simulations (Englmaier & Shlosman 2000). We derive a HCN(4–3) inflow rate of 0.3 $M_\odot$ yr^{-1} at 100 pc, and 0.09 $M_\odot$ yr^{-1} at 40 pc from the SMBH (see Figure 4). The marginal stability criterion of Romeo (1994) ensures that if the gas reaches higher densities, it will be confined to a thinner disk. Hence, changing the gas

density by two orders of magnitude will not change the mass inflow rate (Figure 3). However, accounting for the minimum density variation (arm versus inter-arm) derived from the [S II] line ratios (i.e., $\delta\rho = 5\%$), the inflow rate would decrease by a factor of two (Figure 4).

The critical value $0.01\,\dot{M}_{\rm Edd}$ for the transition between LINER and Sy1 galaxies was found by Ho (2005) with over three orders of magnitudes distribution. The value that we have calculated here for the dense gas streaming, at 40 pc distance from the SMBH in NGC 1097, corresponds to $\dot{M} \sim 0.033\ \dot{M}_{\rm Edd}$, where the Eddington accretion rate is onto a SMBH mass of $1.2 \times 10^8\ M_\odot$ (based on the central stellar velocity dispersion adopted from Lewis & Eracleous (2006) and the $M_\bullet$–σ relation of Tremaine et al. (2002)).

6. CONCLUSIONS

We have presented a detailed kinematics analysis of the dense interstellar gas in the circumnuclear region of the nearby Seyfert 1 galaxy NGC 1097. We used ALMA Band 7 high-resolution observations of the HCN(4–3) emission line, which is postulated to trace $n_{\rm H_2} \sim 10^8$ cm^{-3} at 40 K kinetic temperature. While visual signatures of a rotation pattern dominate the observed velocity field, we have successfully applied Fourier decomposition of the velocity field to unveil the kinematic signatures of two prominent spiral arms (in morphology). The number of nuclear spiral arms in NGC 1097 has been subject to controversy and in the past years it has been clear that the presence of strong obscuration by dust at the very center of this galaxy has complicated matters. We argue here that using velocity information from HCN(4–3) clarifies matters in an unprecedented way.

We have found a striking agreement between the kinematics of HCN(4–3) and an analytic spiral model that we previously built using ionized gas kinematic data at similar spatial resolution. The new ALMA data confirm that the spiral arms have a pitch angle of $52^\circ \pm 4^\circ$, down to $\lesssim$40 pc from the SMBH in NGC 1097.

We note that some studies have found that the HCN molecule could arise from radiation and vibrational excitation (Lepp & Dalgarno 1996; Imanishi et al. 2004; Meier & Turner 2012). The relative contribution of the radiation pumping could then decrease the gas density with which the HCN is associated, and we note that an assumed decrease in density by two orders of magnitudes will yield $h/R < 0.01$. For a thin disk, we have then measured the mass inside the 100 pc radius to be $3.5^{+1.6}_{-2.0} \times 10^8\ M_\odot$, and inside the 40 pc radius, $8.0^{+2.9}_{-3.5} \times 10^6\ M_\odot$. The derived mass at 40 pc agrees with the $<3.0 \times 10^7\ M_\odot$, derived from the observed line flux following the procedure described in Gao & Solomon (2004).

We have used a constant arm versus inter-arm overdensity of 10% and kinematically derived a dense gas inflow of 0.3 $M_\odot$ yr^{-1} at 100 pc and 0.09 $M_\odot$ yr^{-1} at 40 pc radius. In combination with our previously derived values from the ionized and CO gas, we calculate a molecular and ionized gas infall of 0.6 $M_\odot$ yr^{-1} at 100 pc and $\sim$0.2 $M_\odot$ yr^{-1} at 40 pc distance from the central SMBH of NGC 1097. This inflow corresponds to $\dot{M} \sim 0.066\,\dot{M}_{\rm Edd}$ onto a black hole in NGC 1097 with a mass of $1.2 \times 10^8\ M_\odot$. From the current data, it is not clear how much, if any at all, of the observed HCN(4–3) is radiationally excited by the active nucleus. In the presence of radiational excitation, the dense gas scale height that we present here will be lower limits. Notwithstanding, the gas inflow rates remain unchanged.

We thank the referee for improving our manuscript. This Letter makes use of the following ALMA data: ADS/JAO.ALMA#2011.0.00108.S. ALMA is a partnership of ESO, NSF (USA), and NINS (Japan), together with NRC (Canada) and NSC and ASIAA (Taiwan), in cooperation with the Republic of Chile. The Joint ALMA Observatory is operated by ESO, AUI/NRAO, and NAOJ. The NRAO is a facility of the National Science Foundation operated under cooperative agreement by Associated Universities, Inc. Martín is cofunded under Marie Curie Actions of the EC (FP7-COFUND). Matsushita is supported by NSC 100-2112-M-001-006-MY3 of Taiwan. Fathi acknowledges support from the Swedish Research Council & the Swedish Royal Academy of Sciences' Crafoord Prize Foundation.

REFERENCES

Choi, M., Evans, N. J., II, Tafalla, M., & Bachiller, R. 2000, ApJ, 538, 738
Davies, R. I., Maciejewski, W., Hicks, E. K. S., et al. 2009, ApJ, 702, 114
Dicaire, I., Carignan, C., Amram, P., et al. 2008, MNRAS, 385, 553
Englmaier, P., & Shlosman, I. 2000, ApJ, 528, 677
Fathi, K., Storchi-Bergmann, T., Riffel, R. A., et al. 2006, ApJL, 641, L25
Fathi, K., van de Ven, G., Peletier, R. F., et al. 2005, MNRAS, 364, 773
Gao, Y., & Solomon, P. M. 2004, ApJS, 152, 63
Ho, L. C. 2005, Ap&SS, 300, 219
Hsieh, P-Y., Ho, P. T. P., Kohno, K., Hwang, C.-Y., & Matsushita, S. 2012, ApJ, 747, 90
Hsieh, P-Y., Matsushita, S., Lim, J., Kohno, K., & Sawada-Satoh, S. 2008, ApJ, 683, 70
Hsieh, P-Y., Matsushita, S., Liu, G., et al. 2011, ApJ, 736, 129
Imanishi, M., Nakanishi, K., Kuno, N., & Kohno, K. 2004, AJ, 128, 2037
Izumi, T., Kohno, K., Martin, S., et al. 2013, PASJ, submitted
Kohno, K., Ishizuki, S., Matsushita, S., Vila-Vilaró, B., & Kawabe, R. 2003, PASJ, 55, L1
Kohno, K., Kawabe, R., Tosaki, T., & Okumura, S. K. 1996, ApJL, 461, L29
Lepp, S., & Dalgarno, A. 1996, A&A, 306, L21
Lewis, K. T., & Eracleous, M. 2006, ApJ, 642, 711
Lou, Y.-Q., Yuan, C., Fan, Z., & Leon, S. 2001, ApJL, 553, L35
Meier, D. S., & Turner, J. 2012, ApJ, 755, 104
Ondrechen, M. P., van der Hulst, J. M., & Hummel, E. 1989, ApJ, 342, 39
Peebles, P. J. E. 1972, ApJ, 178, 371
Piñol-Ferrer, N., Fathi, K., Carignan, C., et al. 2013, MNRAS, submitted
Piñol-Ferrer, N., Fathi, K., Lundgren, A. A., & van de Ven, G. 2011, MNRAS, 414, 529
Regan, M. W., & Teuben, P. 2003, ApJ, 582, 723
Romeo, A. 1994, A&A, 286, 799
Sakamoto, K., Aalto, S., Evans, A. S., Wiedner, M. C., & Wilner, D. J. 2010, ApJL, 725, L228
Schwarz, M. P. 1984, MNRAS, 209, 93
Sheth, K., & Teuben, P. J. 1999, Natur, 397, 298
Storchi-Bergmann, T., Baldwin, J. A., & Wilson, A. S. 1993, ApJL, 410, L11
Storchi-Bergmann, T., Nemmen da Silva, R., Eracleous, M., et al. 2003, ApJ, 598, 956
Takakuwa, S., Ohashi, N., Bourke, T. L., et al. 2007, ApJ, 662, 431
Tremaine, S., Gebhardt, K., Bender, R., et al. 2002, ApJ, 574, 740
Valotto, C., & Giovanelli, R. 2004, AJ, 128, 115
van de Ven, G., & Chang, P. 2009, ApJ, 697, 619
van de Ven, G., & Fathi, K. 2010, ApJ, 723, 767 (vdVF)
Wong, T. 2000, PhD thesis, Univ. California, Berkeley
Yuan, C., & Yang, C-C. 2006, ApJ, 644, 180